

Electronics and Optics of Graphene Nanoflakes: Edge Functionalization and Structural Distortions

Caterina Cocchi,^{*,†,‡} Deborah Prezzi,^{*,†} Alice Ruini,^{†,‡} Marilia J. Caldas,[¶] and
Elisa Molinari^{†,‡}

*Centro S3, CNR-Istituto Nanoscienze, I-41125 Modena, Italy, Dipartimento di Fisica, Università
di Modena e Reggio Emilia, I-41125 Modena, Italy, and Instituto de Física, Universidade de São
Paulo, 05508-900 São Paulo, SP, Brazil*

E-mail: caterina.cocchi@unimore.it; deborah.prezzi@unimore.it

*To whom correspondence should be addressed

[†]Centro S3, CNR-Istituto Nanoscienze, I-41125 Modena, Italy

[‡]Dipartimento di Fisica, Università di Modena e Reggio Emilia, I-41125 Modena, Italy

[¶]Instituto de Física, Universidade de São Paulo, 05508-900 São Paulo, SP, Brazil

Abstract

The effects of edge covalent functionalization on the structural, electronic and optical properties of elongated armchair graphene nanoflakes (AGNFs) are analyzed in detail for a wide range of terminations, within the framework of Hartree-Fock-based semi-empirical methods. The chemical features of the functional groups, their distribution and the resulting system symmetry are identified as the key factors that determine the modification of structural and optoelectronic features. While the electronic gap is always reduced in presence of substituents, functionalization-induced distortions contribute to the observed lowering by about 35-55%. This effect is paired with a red shift of the first optical peak, corresponding to about 75% of the total optical gap reduction. Further, the functionalization pattern and the specific features of the edge-substituent bond are found to influence the strength and the character of the low energy excitations. All these effects are discussed for flakes of different width, representing the three families of AGNFs.

Keywords: ZINDO, AM1, substitution, UV-vis spectrum, graphene nanoribbons, configuration interaction

The electronic,¹⁻⁴ optical⁵⁻⁷ and magnetic properties⁸⁻¹⁰ of graphene nanoribbons are closely related to their edge morphology and indeed several theoretical proposals have been advanced to tune the properties of these systems through edge modifications. For instance, the termination of edge C atoms with different groups¹¹⁻¹⁴ and the introduction of magnetic impurities¹⁵⁻¹⁸ at the edges of zigzag graphene nanoribbons represent promising routes to fully exploit their potential for spintronics applications. In armchair graphene nanoribbons (AGNRs), on top of the intrinsic tunability given by the well-established family behavior,^{2,3} edge modifications can further engineer the energy gap and work function,¹⁹⁻²³ as well as their optical response.²⁴⁻²⁶

An additional aspect of edge modifications is related to the appearance of structural distortions: ripples and twists can arise, either localized at the edge region^{27,28} or extended to the whole structure, with effects on a larger scale.²⁹⁻³¹ Indeed, the study of structural modifications has drawn itself great attention, since they can lead to a further tuning of the graphene nanostructure properties.^{32,33} We here focus on unraveling the effects of functionalization-induced structural, electronic and optical modifications, considering not only the functional group itself but also the functionalization pattern. Such analysis can be particularly relevant to design new optoelectronic functionalities in graphene nanostructures, above all in light of the recent improvements in their controlled synthesis at the nanoscale.³⁴⁻⁴⁰

We carry out our analysis on short armchair graphene ribbons functionalized with different edge-substituents, ranging from single atoms to small molecular moieties. Family-dependence is also taken into account. We recognize that several factors –including the system symmetry, the chemical features of the functional groups and their distribution– are responsible for the appearance of different structural and optoelectronic modifications. In general, the steric hindrance of substituents is found to induce local distortions at the edges, but global effects involving the flake backbone can also arise in specific cases. These structural modifications are found to reduce the electronic gap up to 300 meV, corresponding to 55% of the total gap decrease. This effect is associated to a similar red-shift of the first optical peak. On the other hand the chemical features of the substituents and their arrangement at the edges crucially influence the distribution of the frontier

orbitals. Local variations arise as a consequence of the modified molecular symmetry upon edge functionalization, while global localization effects are noticed when a large longitudinal dipole component is introduced by polar substituents. Moreover, such charge redistribution results in the appearance of an additional peak in the low energy region of the spectra, related to the optical activation of an otherwise dark excitation.

Methods and System Description

The results presented in this paper are obtained within the framework of Hartree-Fock based semi-empirical methods,⁴¹ which are well tested and reliable for the evaluation of the electronic and optical properties of C-conjugated low-dimensional systems.^{42–45} The AM1 model⁴⁶ is adopted for structural optimization (0.4 kcal · mol⁻¹/Å threshold for the forces) and for the study of the electronic properties, including the calculation of electric dipole moments. The electronic gap is computed as the difference between *vertical* ionization potential (IP) and electron affinity (EA), which are in turn obtained from the total energy of the neutral and (± 1) charged states, i.e. IP = E(+1) - E(0) and EA = E(0) - E(-1). The optical spectra are evaluated by means of the ZINDO/S model,⁴⁷ with single excitation Configuration Interaction (CIS). Our convergence tests over the number of occupied and virtual molecular orbitals (MOs) indicated that a CI energy window of at least 4.5 eV below the HOMO and 3.5 eV above the LUMO is required for a reliable characterization of the low energy optical excitations.

We perform our analysis on elongated graphene nanoflakes (GNFs) with armchair-shaped edges, which can be seen as finite portions of graphene nanoribbons. As for infinite ribbons, we introduce a width parameter N , corresponding to the number of dimeric C lines across the y axis (see 1a). According to their width parameter N , both ribbons^{2,3} and flakes²³ present three scaling laws for the energy gap, also in presence of edge substituents. This allows us to classify them into three different families, following a *modulo 3* periodic law: $N = 3p + m$, with p integer and $m = 0, 1, 2$. In the following, we will mainly focus on a $N = 7$ GNF (width ~ 7.3 Å) of length ~ 24 Å (x axis,

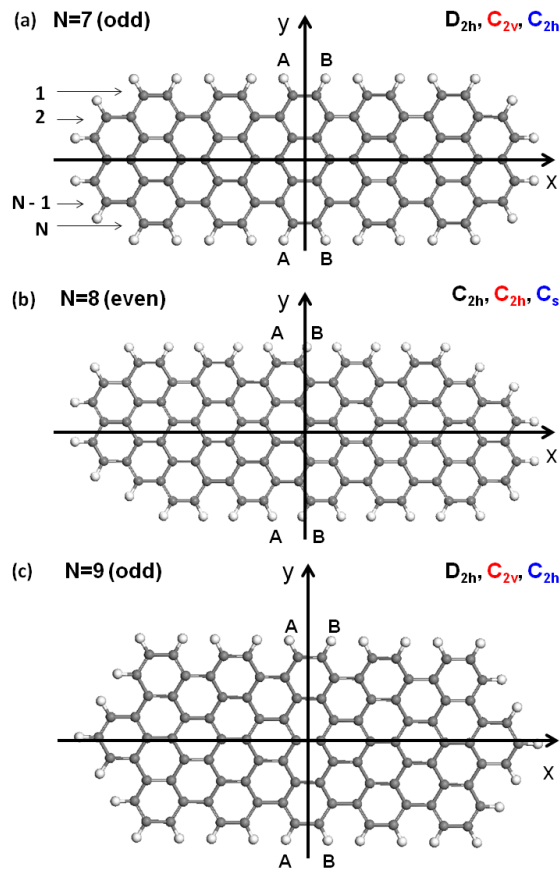


Figure 1: H-terminated armchair graphene nanoflakes (AGNFs) of fixed length (x axis) and variable width (y axis), chosen as representative of the three different families of AGNFs, i.e. $N=3p$, $3p+1$ and $3p+2$. Edge functionalization is performed by replacing each second H atom along the length with a foreign substituent. Two functionalization schemes can be identified: the A-A scheme, where the same zigzag line is functionalized on both edges, and the A-B scheme, where functionalization involves alternating zigzag lines. Indicated are the point symmetry groups of each structure, clean (black), and functionalized in the A-A (red) and A-B (blue) scheme, respectively, for ideal (non-distorted and symmetrically terminated) flakes.

see 1a). We will then extend our analysis to the family dependence by considering two additional structures (shown in 1b-c), having widths 8.6 Å ($N=8$) and 9.8 Å ($N=9$) and fixed length. For each structure, the lateral ends along the x axis are shaped in such a way to minimize the influence of zigzag edges, which are known to affect the electronic properties of the system.^{48,49}

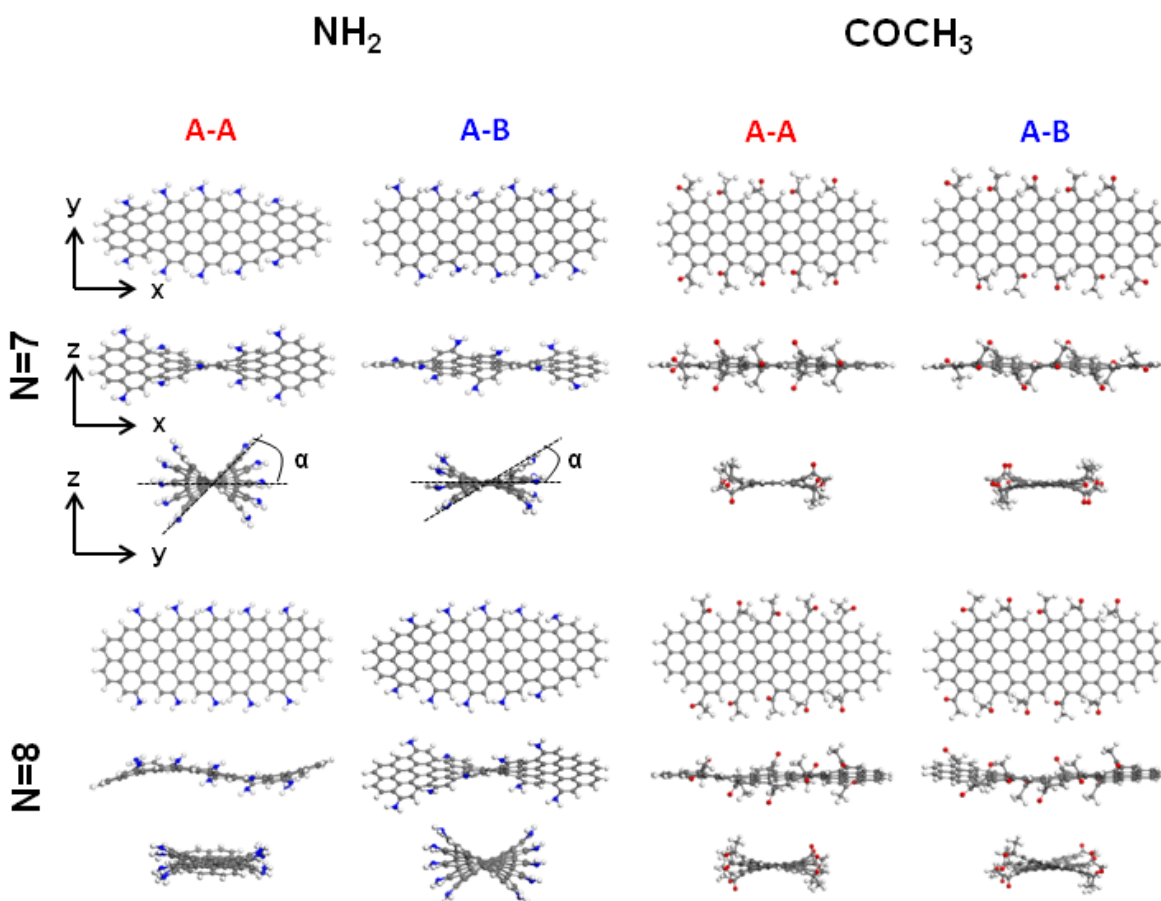


Figure 2: Structurally optimized $N=7$ and $N=8$ AGNFs, functionalized with NH_2 (left) and COCH_3 (right) groups, according to the A-A and A-B schemes. The angle α is introduced to quantify the distortion angle, defined as the maximum deviation from planarity of edge C atoms.

The effects of edge substituents on the electronic and optical properties of GNFs are investigated for a number of light-element metal-free functional groups, including atoms and molecular groups typically involved in electrophilic aromatic substitutions.^{50,51} We group these terminations into three main classes, with respect to the nature of their covalent bond with the graphene edge: the first class comprises monovalent halogen terminations (F, Cl and Br); the second consists of

groups forming a direct bond at the edge, in which either N or O shares a $2p$ lone pair with the edge C atom (NH_2 , OCH_3 and $\text{OCF}=\text{CF}_2$); as a third class, we finally consider small moieties bonded to the GNF through a C-bond and including a C-double bond, which allows to extend the C-conjugation of the graphene backbone for one additional bond length beyond the edge (COCH_3 , $\text{CH}=\text{CH}_2$ and $\text{CH}=\text{CF}_2$). The choice of these terminations is basically motivated by their experimental feasibility in systems similar to those investigated here.^{34,52–54}

Edge covalent functionalization is here performed by replacing each second H atom passivating the armchair edges in the reference system, through the regular alternation of substituents. As indicated in 1, two functionalization schemes can be designed: in the A-A scheme the same C zigzag line is functionalized on opposite edges, while in the A-B scheme alternating C zigzag lines are functionalized. In addition, full substitution, i.e. functionalization of all C edge atoms, is considered for monoatomic halogen terminations only, as justified by their reduced size. Note that, depending on the chosen scheme and on the flake width, each structure has different symmetry. H-terminated flakes have D_{2h} (C_{2h}) symmetry for N odd (even), which is modified by the presence of functional groups at the edges. For N odd, the A-A scheme results in a C_{2v} symmetry, while in the A-B scheme the symmetry is C_{2h} . On the contrary, for N even the symmetry is preserved as C_{2h} in the A-A scheme and lowered to C_s in the A-B scheme. Even though this classification is formally correct only for ideal non-distorted and symmetrically terminated structures, since the symmetry is always lowered upon structural optimization, we will keep this notation throughout the paper for convenience.

Results and Discussion

Edge covalent functionalization is known to be an effective strategy to tune the electronic gap of graphene nanostructures.^{19,20,22,32} As suggested already for simple aromatic compounds,^{55–57} the presence of edge functional groups modifies the electronic distribution within the graphene network in the edge proximity. As a consequence, heterospecies with different electronegativity

than C and covalently bonded at the edges of a graphene ribbon allow to modify the ionization potential (IP) and the electron affinity (EA) of the system with respect to the reference H-passivated flake.²³ The optical characteristics are then directly affected.²⁶ However, the edge-decoration of the flakes induces also structural modifications, which are closely related and interdependent with the electronic stabilization, as we will see in the following.

2 shows that, depending on the value of N (even or odd), the type of substituent and the functionalization scheme (A-B or A-A), different types of distortions can arise, either localized at the edges or extended to the flake backbone. For instance, for COCH_3 we have a typical case of structural modifications mostly localized at the edges: there is a slight difference for different N and scheme, however there are no global, coherent modifications. In this case, local steric effects among the functional groups play a primary role in driving distortions: COCH_3 groups, which can reorient to minimize the repulsion, induce relatively small tilt of edge C rings to opposite directions, perpendicular to the flake basal plane (z axis, see 2). As a second example, we highlight the case of the NH_2 termination: here the interplay of functionalization pattern, group rigidity and steric effects can produce coherent distortions involving the whole flake backbone, which thus stabilize the structure. This is evident for $N=7$ ($N=8$) in the A-A (A-B) scheme (2), where the system tends to twist along its longitudinal axis (x). For $N=8$ in the A-A scheme, a “rippling” mode tends also to appear on top of the local distortions induced at the edges.

To quantify these effects, we introduce an angle α , defined as the maximum deviation of edge C atoms with respect to the reference planar configuration (H-GNF, $\alpha=0$). The values of α for different functional groups are reported in 1 for $N=7$ GNFs (see Supporting Information for $N=8$ and $N=9$, Table S3). In the case of halogen termination, similar distortion angles are observed for both A-A and A-B schemes, while a significantly larger tilting angle is produced upon full functionalization. For molecular substituents, where larger distortions are expected in view of their size, the tilt of edge C-rings is considerably reduced when the groups are relatively free to rearrange, as we described for COCH_3 . This is also the case of methoxy (OCH_3) and $\text{OCF}=\text{CF}_2$ groups, where the flexible O-linkage allows them to assume an ordered alignment (see Supporting

Information, Figure S1). On the contrary, larger α angles (and global distortions) are noticed for rigid groups like NH_2 and ethene units ($\text{CH}=\text{CF}_2$ and $\text{CH}=\text{CH}_2$). We remark finally that, even when we find discernible structural modifications, they do not result in any significant local deviation from the regular graphene bonding and no strongly localized defects appear. For further structural details (edge C-C and C-substituent bond lengths), see Supporting Information, Table S1-S2.

Table 1: Distortion angles α (in degrees) for $N=7$ GNFs functionalized according to the indicated schemes (1st column). The angle α indicates the maximum deviation of edge C atoms as compared to the reference planar H-GNF, as shown in 2.

	Halogen			Direct bond			C bond		
	F	Cl	Br	NH_2	OCH_3	$\text{OCF}=\text{CF}_2$	COCH_3	$\text{CH}=\text{CF}_2$	$\text{CH}=\text{CH}_2$
A-A	7.2	11.3	12.0	36.5	11.1	22.2	10.5	19.2	25.3
A-B	6.6	10.6	12.5	22.8	8.7	15.3	12.5	26.2	15.5
full	17.1	31.3	29.1	-	-	-	-	-	-

We now move to the electronic properties and list in 2 the total dipole arising in presence of different substitution patterns. We notice that a large dipole along the flake longitudinal axis (x) appears for N odd (here $N=7$) in the A-A functionalization scheme, while it is almost negligible for the other scheme. The situation is reversed for N even (e.g. $N=8$, see Supporting Information, Table S4). As shown in 2 and in 3a, the dipole orientation and intensity depend on the characteristics of the functional group: electron-donating (e.g. NH_2) and -withdrawing groups (e.g. F and COCH_3) produce large longitudinal dipoles oriented in opposite directions (see also 3a). The presence of a sizeable longitudinal dipole (A-A pattern for $N=7$ GNF) is accompanied by a spatial localization of the frontier orbitals on opposite sides of the flake. As depicted in 3b, for $\mu_x \neq 0$ the potential well describing the flake assumes a “saw-tooth” profile (see e.g. Ref.⁵⁸), whose height and orientation depends on the magnitude and on the sign of μ_x . Hence the HOMO and LUMO states present a similar asymmetric character in both cases, but with spatially opposite localization (see 3b). On the other hand, for the A-B scheme the π distribution of the frontier orbitals undergoes only local modifications, specifically related to the altered symmetry of the flake,⁵⁹ as shown in 3c. The modified symmetry of the frontier orbitals is particularly evident for the NH_2 termination, while it

is less apparent for groups bonded through a C bond, such as COCH_3 . See Supporting Information for a more complete analysis of the substituents and family dependence (Figure S1-S2).

Table 2: Components of the dipole moment for edge-functionalized $N=7$ GNFs (one substituent per class), according to the A-A and A-B functionalization schemes.

Group	Scheme	μ_x [D]	μ_y [D]	μ_z [D]
F	A-A	4.848	0.479	0.028
	A-B	-0.001	-0.003	-0.061
NH_2	A-A	-9.335	-0.026	-0.121
	A-B	0.339	-1.238	3.823
COCH_3	A-A	9.764	1.138	-0.049
	A-B	0.166	-0.139	0.269

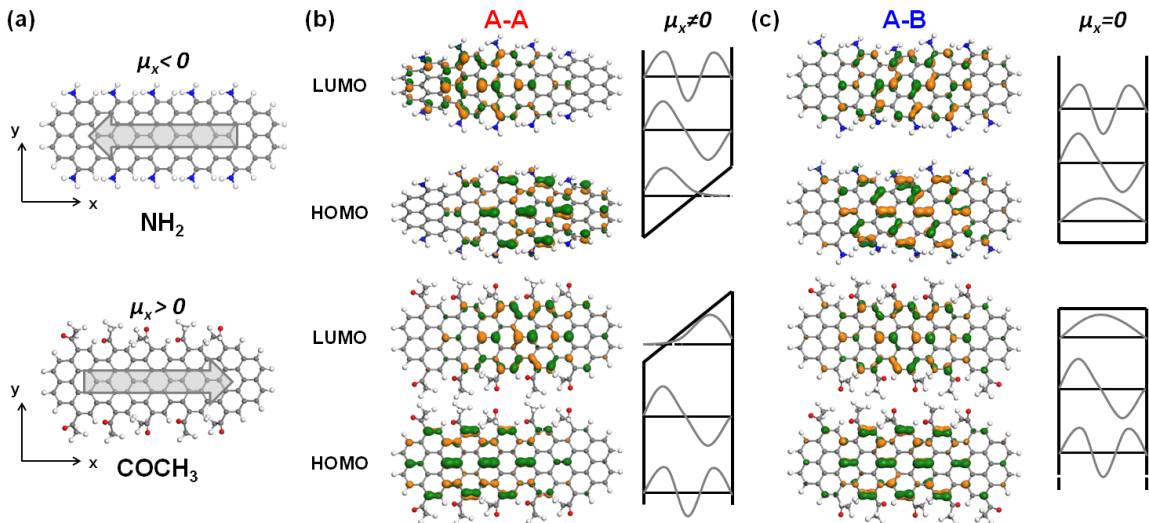


Figure 3: (a) A-A functionalization of $N=7$ GNF by means of electron-donating (e.g. NH_2) and -withdrawing (e.g. COCH_3) groups gives rise to longitudinal dipoles (μ_x) oriented in opposite directions. The frontier orbitals of NH_2 - and COCH_3 -substituted $N=7$ GNFs are shown for the (b) A-A and (c) A-B schemes. The square well potential profiles modulating the molecular orbital distribution are sketched in presence (b) and absence (c) of a longitudinal dipole along the flake.

In 3 we report the differences of IP and EA (ΔEA and ΔIP) of $N=7$ functionalized GNFs with respect to the reference hydrogenated flake, as well as their energy gap (E_G). As expected, an uneven shift of IP and EA is produced upon functionalization, related to the electronegativity of the substituents; for instance, highly electronegative halogen terminations upwards shift EA more significantly than IP, while strongly electron-donating amino groups downwards move IP more

Table 3: Differences of EA and IP (ΔEA and ΔIP , in eV) with respect to the reference hydrogenated (H) flake and energy gap (E_G , in eV) computed through AM1 model for $N=7$ GNFs, functionalized according to the A-B scheme. For selected groups, we report the values of ΔEA , ΔIP and E_G also for the A-A scheme and for H-terminated model flakes with the corresponding distorted geometries (in italics).

	H	Halogens				Direct bond				C-bond			
		F		Cl	Br	NH ₂		OCH ₃	OCF=CF ₂	COCH ₃		CH=CF ₂	CH=CH ₂
		A-A	A-B			A-A	A-B			A-A	A-B		
ΔEA	0.00	0.57 <i>0.01</i>	0.58 <i>0.01</i>	0.53	0.62	-0.18 <i>0.08</i>	-0.14 <i>0.04</i>	-0.12	0.70	0.74 <i>0.01</i>	0.69 <i>0.01</i>	0.67	0.14
ΔIP	0.00	0.37 <i>-0.10</i>	0.32 <i>-0.10</i>	0.30	0.39	-0.75 <i>-0.24</i>	-0.79 <i>-0.19</i>	-0.50	0.31	0.49 <i>-0.10</i>	0.42 <i>-0.10</i>	0.19	-0.22
E_G	5.13	4.92 <i>5.01</i>	4.87 <i>5.01</i>	4.90	4.90	4.55 <i>4.81</i>	4.47 <i>4.90</i>	4.75	4.74	4.88 <i>5.01</i>	4.86 <i>5.01</i>	4.65	4.76

than EA. In any case, a gap reduction is always encountered. In the case of C-bonded terminations, a further contribution to the gap reduction is given by the increased effective width of the flake, driven by the extended π -conjugation.

In addition to this well-established behavior, we here more directly estimate the role played by structural distortions. To quantify this effect, we consider model flakes obtained by removing the functionalizing groups from the final structure, and by then H-passivating the remaining dangling bonds: this model structure allows us to decouple the influence of distortions from the overall influence of edge functionalization. By inspecting 3, we find a total gap reduction upon functionalization ranging from 200 to 700 meV. The comparison with the values of E_G obtained for the model distorted H-GNFs (in italics in 3) points to a non-negligible contribution of structural distortions, corresponding to 35-55% of the total amount. These results are very similar to what expected for thermal deviations from the ideal structure.⁶⁰ It is also worth noting that this trend is mostly independent of the functionalization scheme, with a maximum difference of 80 meV for the NH₂ case, where the two schemes induce significantly different distortion patterns.

Starting from the AM1 results described above, we now turn to the analysis of optical excitations, as obtained from ZINDO calculations. To address the role of both molecular-symmetry and structural modifications, we first consider the $N=7$ GNF functionalized with NH₂, where these

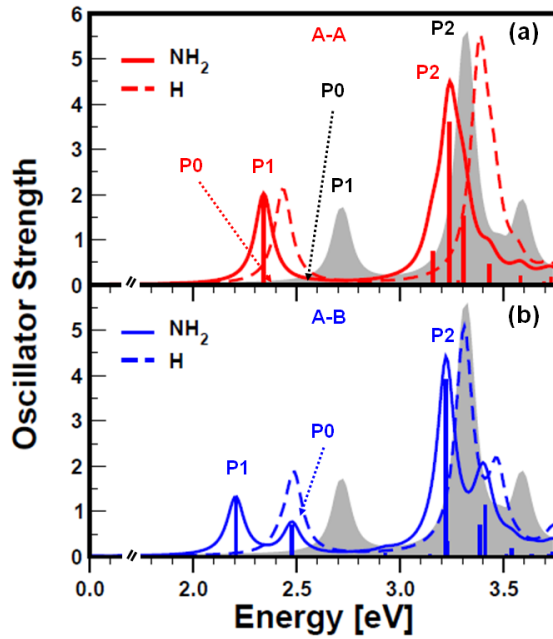


Figure 4: Optical spectra of GNFs of width parameter $N=7$, functionalized with NH_2 groups, according to the (a) A-A and (b) A-B functionalization schemes. In addition to the spectrum of the planar H-terminated flake taken as reference (grey shaded area, with the main excitations highlighted in a), we show the spectrum of model GNFs obtained by removing the edge substituents from the final structures and H-passivating the dangling bonds (dashed lines), in order to perform a rigorous analysis of distortions effects. All the curves are obtained through a Lorentzian broadening of 50 meV.

effects are both prominent. In 4 we report the optical spectra for both functionalization schemes, A-A (red) and A-B (blue), together with the spectrum of the flat H-GNF (grey shaded area), taken as a reference. In addition, we include the spectrum of the H-terminated distorted model flake described above (dashed line), which enables a direct analysis of the distortion effects. As already discussed,⁶¹ the optical spectrum of the planar $N=7$ H-GNF shows two main peaks in the low-energy region with longitudinal polarization (along the x axis), labelled as P1 and P2; in addition, a transversally polarized weak excitation (P0) is found at lower energy. Our results indicate that edge functionalization is responsible for a red shift of the P1 peak by 380 and 510 meV in the A-A (4a) and A-B schemes (4b), respectively. Remarkably, a further peak is observed in the optical spectrum of the A-B functionalized flake, related to the oscillator strength (OS) increase of P0 by about 3 orders of magnitude. This OS gain is a purely symmetry effect: the molecular symmetry reduction induced by functionalization (from D_{2h} in the H-GNF to C_{2h} in the A-B scheme) implies that the HOMO state acquires the same symmetry as the HOMO-1 one, so that the HOMO \rightarrow LUMO transition is now allowed to contribute to the P0 excitation (see 4). This symmetry effect is in fact not observed in the A-A functionalized flake.

Concerning the role of structural distortion, we observe that the largely distorted geometry produced by the A-A functionalization (dashed line in 4a) is responsible for about 75% of the optical gap reduction, as noticed by comparing the excitation energy of P1 for the three curves in 4a. P1 is now energetically degenerate with the dark excitation P0, also red shifted of about 200 meV with respect to the reference H-GNF (see 4). It is worth noting that the frontier orbital localization observed for the A-A scheme in presence of polar functional groups (see 3b) does not affect the basic features of the main excitations: despite their spatial localization, the overlap between the frontier orbitals is still large enough to preserve the intensity of P1, in comparison with both the reference H-terminated and the A-B functionalized GNF. In the case of the A-B functionalization pattern, distortions contribute to about 45% of the whole optical gap red shift: the impact of distortions is less pronounced for this structure, and molecular symmetry effects dominate (see 4b).

We next inspect the role of the chemical specificities of edge substituents, by comparing the

Table 4: Energy, oscillator strength (OS) and composition in terms of molecular orbital transitions of the main excitations of functionalized $N=7$ GNFs, in presence of one prototypical substituent per class, i.e. F, NH_2 (also A-A scheme) and COCH_3 , in addition to the reference hydrogenated system. In the last column we report the MO transitions contributing to each excitation which have a relative weight larger than 0.1

Termination	Excitation	Energy [eV]	OS	Transitions (weight)
H	P0	2.54	0.0005	H-1 \rightarrow L (0.37) H \rightarrow L+1 (0.39)
	P1	2.72	1.62	H \rightarrow L (0.79)
	P2	3.32	5.43	H-3 \rightarrow L+3 (0.12) H-1 \rightarrow L+1 (0.76)
F	P0	2.43	0.21	H-1 \rightarrow L (0.27) H \rightarrow L (0.12) H \rightarrow L+1 (0.37)
	P1	2.58	1.54	H \rightarrow L (0.68)
	P2	3.26	5.11	H-3 \rightarrow L+3 (0.20) H-1 \rightarrow L+1 (0.71)
NH_2 - A-A	P1	2.34	1.98	H \rightarrow L (0.75)
	P0	2.35	0.02	H-2 \rightarrow L (0.29) H \rightarrow L+1 (0.39)
	P2	3.24	3.59	H-2 \rightarrow L+1 (0.50)
NH_2 - A-B	P1	2.21	1.29	H \rightarrow L (0.63)
	P0	2.48	0.70	H-2 \rightarrow L (0.22) H \rightarrow L (0.18) H \rightarrow L+1 (0.40)
	P2	3.22	3.92	H-2 \rightarrow L+1 (0.53) H \rightarrow L+1 (0.10)
COCH_3	P0	2.42	0.04	H-1 \rightarrow L (0.34) H \rightarrow L+1 (0.40)
	P1	2.55	1.68	H \rightarrow L (0.78)
	P2	3.21	5.13	H-1 \rightarrow L+1 (0.71)

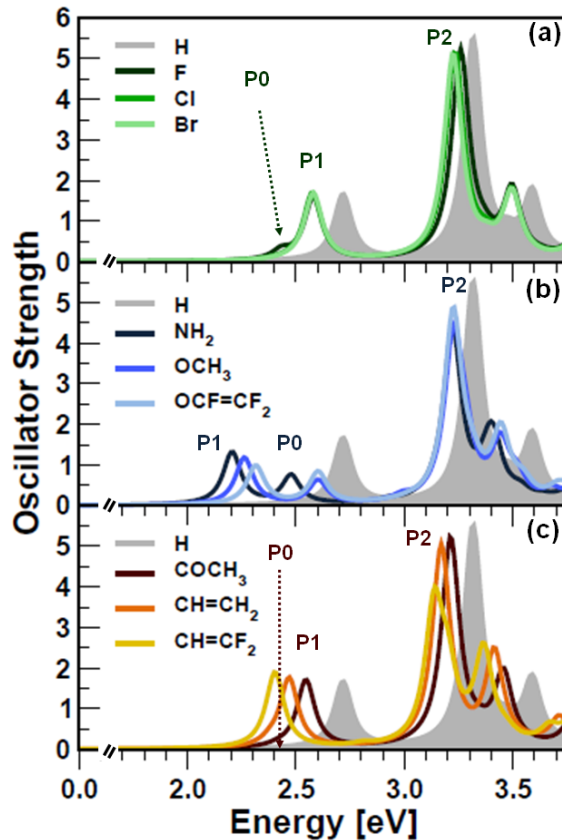


Figure 5: Optical spectra N=7 GNFs functionalized in the A-B scheme with each terminations considered in this work, including (a) halogen atoms, (b) directly- and (c) C-bonded groups. In each panel, we indicate for one of the groups the three main excitations described in the text, i.e. P0, P1 and P2. Moreover, the spectrum of the reference H-flake is reported (grey shaded area in each panel). All the curves are obtained through a Lorentzian broadening of 50 meV.

optical spectra of $N=7$ GNFs functionalized with all the anchoring groups considered in this work, as shown in 5. We here consider only the A-B pattern, since negligible differences are observed between the two schemes for most of the substituents (see Figure S3 in the Supporting Information for more details). The analysis of fully halogen terminated GNFs is also included in the Supporting Information (see Figure S4 and Table S8). A non rigid red shift of the spectra is generally observed upon functionalization, with a larger red shift for P1 than for P2. All the spectra of the groups anchored through a direct bond (5b) display the same key feature already discussed for the amino termination and reported in 4b: an additional distinct peak emerges, corresponding to the P0 excitation which becomes optically active. This effect is also present, even though less intense, for halogen terminations: P0 appears as a shoulder in the main P1 peak for fluorinated flakes (5a). In the case of C-bonded molecular substituents, the impact of functionalization on the electronic states is further reduced, so that the main spectral features are basically preserved with respect to the flat H-terminated flake (see spectra in 5b and the composition of the main excitations in 4).

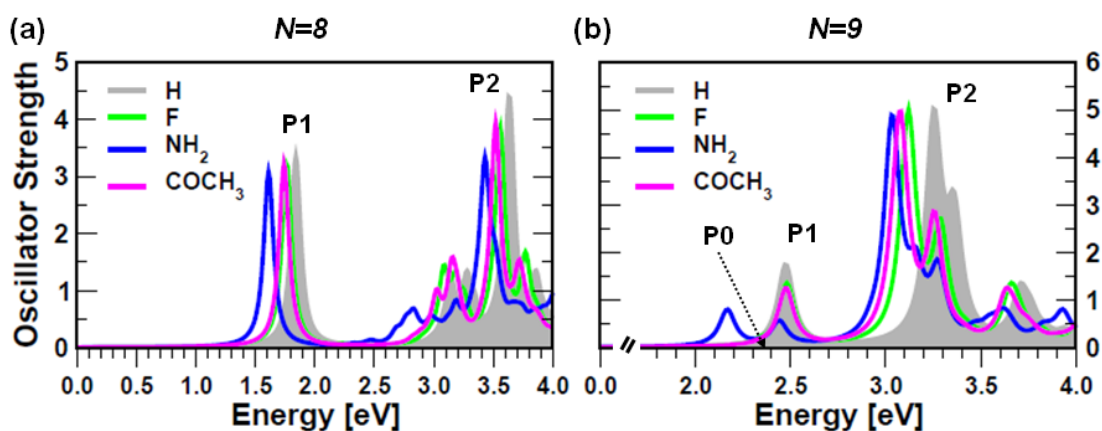


Figure 6: Optical spectra of symmetrically functionalized GNFs of width parameter (a) $N=8$ (A-A scheme) and (b) $N=9$ (A-B scheme). One edge substituent for each class of terminations considered in this work is addressed for both GNFs. The spectrum of the reference H-GNF is reported in the background of each panel (grey shaded area) with the indication of the main excitations (P0, P1 and P2). All the curves are obtained through a Lorentzian broadening of 50 meV.

In order to complete our analysis, we finally investigate the spectra of the GNFs of width parameter $N = 8$ and $N = 9$, functionalized with one prototypical group per class, namely F, NH_2

and COCH_3 , according to the higher symmetry scheme (A-A for $N=8$ and A-B for $N=9$). The optical spectra computed for these systems are shown in 6, with the reference spectrum of the corresponding planar H-GNF reported in the background of each panel (grey shaded area). The optical spectrum of the $N=8$ GNF is dominated by a first intense peak P1, which is about 1 eV lower in energy compared to those of the other GNF families (compare 6a with 5 and 6b), in agreement with the trend for the electronic gaps.²³ Contrary to $N=7$, this is always the lowest energy excitation, regardless the edge termination (See Supporting Information, Table S5). Moreover, we do not observe any functionalization-induced modification in the π distribution of frontier orbitals, since the molecular symmetry remains the same in the A-A scheme (C_{2h}). In this case the main effect of functionalization is thus to red shift the spectrum with respect to the reference H-GNF, in an almost rigid fashion (up to over 200 meV upon amino termination).

On the other hand, the optical spectra of $N=9$ GNFs manifest more similarities with those of $N=7$ GNFs (see 6b and 5 for comparison), both in the spectral shape and in the composition of the main excitations (see Supporting Information, Table S6). Also for the ribbons belonging to the $N=3p$ family, the P0 excitations becomes optically active, giving rise to a distinct peak in presence of NH_2 functional groups, according to the mechanism described for the $N=7$ GNFs. The lowest energy peak is red shifted by about 300 meV upon amino substitution, compared to the reference H-GNF. In presence of other edge substituents (F and COCH_3), the energy of P1 is basically unaffected, while P2 is red shifted of about 200 meV upon each termination (see 6b). This is an effect of the MO distribution observed for the GNFs belonging to this family, for which the frontier orbitals present reversed orientation of the π distribution with respect to the flakes of the $N=3p+1$ family (see Figure S2).

Conclusions

We have analyzed in details the effects of edge covalent functionalization on the structural, electronic and optical properties of armchair graphene nanoflakes. Different functionalization groups

and patterns have been discussed for a specific flake, and the analysis extended and rationalized for additional systems, according to the armchair width modulation. Our results indicate that steric repulsion among substituents generally determines local distortion at the edges, even though structural modifications can involve the whole flake backbone in specific cases. Functionalization-induced distortions are found to play an effective role in the electronic gap reduction experienced by the flakes, with contributions ranging from 35 to 55% of the total gap decrease. Depending on the functionalization pattern and the character of the substituents, interesting charge-redistribution effects are seen for the frontier orbitals, either related to the modified molecular symmetry or to the appearance of a large longitudinal dipole component. All these effects are reflected in the optical spectra: distortions largely contribute to the lowering of the optical gap (up to 300 meV), while the appearance of an additional peak at low energy is related to the distribution and the characteristics of the functional groups. Our results indicate that the interplay among the system symmetry, the chemical features and the distribution of the substituents, as well as the resulting structural distortions is crucial to understand the modification of the opto-electronic properties of functionalized graphene nanoflakes.

Acknowledgement

The authors are grateful to Stefano Corni for fruitful discussion and acknowledge CINECA for computational support. This work was partly supported by the Italian Ministry of University and Research under FIRB grant ItalNanoNet, and by Fondazione Cassa di Risparmio di Modena with project COLDandFEW. M. J. C. acknowledges support from FAPESP and CNPq (Brazil).

Supporting Information Available

The Supporting Information is organized in three sections. In the first one we report the structural details (bond lengths and distortion angles) of the optimized $N=7$, $N=8$ and $N=9$ graphene nanoflakes, to complete the data reported in the main text. The second section supports the analysis on the electronic properties, including a table with the dipole moment components of $N=8$ and $N=9$

GNFs (functionalized according to both A-A and A-B schemes) and the isosurfaces of the frontier orbitals for the considered systems. The last part is dedicated to optical properties. The analysis on the effects related to different functionalization schemes and structural distortions are extended here also to COCH₃ and F terminations, as representatives of the classes of C-bonded and halogen substituents. We also include the tables with the composition of the main excitations for $N=8$ and $N=9$ GNFs, and the analysis of the optical features of full halogen-terminated GNFs (only $N=7$). This material is available free of charge via the Internet at <http://pubs.acs.org/>.

Notes and References

- (1) Castro Neto, A. H.; Guinea, F.; Peres, N. M. R.; Novoselov, K. S.; Geim, A. K. *Rev. Mod. Phys.* **2009**, *81*, 109–162.
- (2) Nakada, K.; Fujita, M.; Dresselhaus, G.; Dresselhaus, M. S. *Phys. Rev. B* **1996**, *54*, 17954–17961.
- (3) Son, Y.-W.; Cohen, M. L.; Louie, S. G. *Phys. Rev. Lett.* **2006**, *97*, 216803.
- (4) Barone, V.; Hod, O.; Scuseria, G. E. *Nano Lett.* **2006**, *6*, 2748–2754.
- (5) Prezzi, D.; Varsano, D.; Ruini, A.; Marini, A.; Molinari, E. *Phys. Rev. B* **2008**, *77*, 041404(R).
- (6) Yang, L.; Cohen, M.; Louie, S. *Nano Lett.* **2007**, *7*, 3112–3115.
- (7) Yang, L.; Cohen, M. L.; Louie, S. G. *Phys. Rev. Lett.* **2008**, *101*, 186401.
- (8) Yazyev, O. *Rep. Prog. Phys.* **2010**, *73*, 056501.
- (9) Pisani, L.; Chan, J. A.; Montanari, B.; Harrison, N. M. *Phys. Rev. B* **2007**, *75*, 064418.
- (10) Son, Y.-W.; Cohen, M. L.; Louie, S. G. *Nature (London)* **2006**, *444*, 347–349.
- (11) Hod, O.; Barone, V.; Peralta, J. E.; Scuseria, G. E. *Nano Lett.* **2007**, *7*, 2295–2299.
- (12) Gunlycke, D.; Li, J.; Mintmire, J. W.; White, C. T. *Appl. Phys. Lett.* **2007**, *91*, 112108.

- (13) Kan, E.-j.; Li, Z.; Yang, J.; Hou, J. G. *J. Am. Chem. Soc.* **2008**, *130*, 4224–4225.
- (14) Wu, M.; Wu, X.; Zeng, X. *J. Phys. Chem. C* **2010**, *114*, 3937–3944.
- (15) Rigo, V.; Martins, T.; da Silva, A.; Fazzio, A.; Miwa, R. *Phys. Rev. B* **2009**, *79*, 075435.
- (16) Longo, R. C.; Carrete, J.; Ferrer, J.; Gallego, L. J. *Phys. Rev. B* **2010**, *81*, 115418.
- (17) Wang, Y.; Cao, C.; Cheng, H. *Phys. Rev. B* **2010**, *82*, 205429.
- (18) Cocchi, C.; Prezzi, D.; Calzolari, A.; Molinari, E. *J. Chem. Phys.* **2010**, *133*, 124703.
- (19) Cervantes-Sodi, F.; Csányi, G.; Piscanec, S.; Ferrari, A. C. *Phys. Rev. B* **2008**, *77*, 165427.
- (20) Ren, H.; Li, Q.; Su, H.; Shi, Q. W.; Chen, J.; Yang, J. *Cond-Mat* **2007**, arXiv0711.1700v1.
- (21) Lu, Y.; Wu, R.; Shen, L.; Yang, M.; Sha, Z.; Cai, Y.; He, P.; Feng, Y. *Appl. Phys. Lett.* **2009**, *94*, 122111.
- (22) Wang, W.; Li, Z. *J. Appl. Phys.* **2011**, *109*, 114308.
- (23) Cocchi, C.; Ruini, A.; Prezzi, D.; Caldas, M. J.; Molinari, E. *J. Phys. Chem. C* **2011**, *115*, 2969–2973.
- (24) Zhu, X.; Su, H. *J. Phys. Chem. C* **2010**, *114*, 17257–17262.
- (25) Prezzi, D.; Varsano, D.; Ruini, A.; Molinari, E. *Phys. Rev. B* **2011**, *84*, 041401.
- (26) Cocchi, C.; Prezzi, D.; Ruini, A.; Caldas, M.; Molinari, E. *J. Phys. Chem. Lett.* **2011**, *2*, 1315–1319.
- (27) Wagner, P.; Ewels, C. P.; Ivanovskaya, V. V.; Briddon, P. R.; Pateau, A.; Humbert, B. *Phys. Rev. B* **2011**, *84*, 134110.
- (28) Rosenkranz, N.; Till, C.; Thomsen, C.; Maultzsch, J. *Phys. Rev. B* **2011**, *84*, 195438.
- (29) Bets, K.; Yakobson, B. *Nano Res.* **2009**, *2*, 161–166.

- (30) Shenoy, V. B.; Reddy, C. D.; Zhang, Y.-W. *ACS Nano* **2010**, *4*, 4840–4844.
- (31) Lu, Q.; Huang, R. *Phys. Rev. B* **2010**, *81*, 155410.
- (32) Peng, X.; Velasquez, S. *Appl. Phys. Lett.* **2011**, *98*, 023112.
- (33) Sadrzadeh, A.; Hua, M.; Yakobson, B. *Appl. Phys. Lett.* **2011**, *99*, 013102.
- (34) Wu, J.; Pisula, W.; Muellen, K. *Chem. Rev.* **2007**, *107*, 718–747.
- (35) Kosynkin, D. V.; Higginbotham, A. L.; Sinitskii, A.; Lomeda, J. R.; Dimiev, A.; Price, B. K.; Tour, J. M. *Nature (London)* **2009**, *458*, 872.
- (36) Jiao, L.; Zhang, L.; Wang, X.; Diankov, G.; Dai, H. *Nature (London)* **2009**, *458*, 877.
- (37) Cai, J.; Ruffieux, P.; Jaafar, R.; Bieri, M.; Braun, T.; Blankenburg, S.; Muoth, A. P.; Matthiasand Seitsonen; Saleh, M.; Feng, X.; Muellen, K.; Fasel, R. *Nature (London)* **2010**, *466*, 470–473.
- (38) Jia, X.; Campos-Delgado, J.; Terrones, M.; Meunier, V.; Dresselhaus, M. *Nanoscale* **2010**, *3*, 86–95.
- (39) Palma, C.; Samorí, P. *Nature Chem.* **2011**, *3*, 431–436.
- (40) Blankenburg, S.; Cai, J.; Ruffieux, P.; Jaafar, R.; Passerone, D.; Feng, X.; MÃĀĀijllen, K.; Fasel, R.; Pignedoli, C. A. *ACS Nano* **2012**, *6*, 2020–2025.
- (41) AM1 and ZINDO/S calculations were performed using VAMP package included in Accelrys Materials Studio software, version 5.0 (<http://accelrys.com/products/materials-studio>).
- (42) Wetmore, S. D.; Boyd, R. J.; Eriksson, L. A. *Chem. Phys. Lett.* **2000**, *322*, 129 – 135.
- (43) Caldas, M. J.; Pettenati, E.; Goldoni, G.; Molinari, E. *Appl. Phys. Lett.* **2001**, *79*, 2505–2507.
- (44) Dávila, L. Y. A.; Caldas, M. J. *J. Comput. Chem.* **2002**, *23*, 1135.

- (45) Kubatkin, S.; Danilov, A.; Hjort, M.; Cornil, J.; Brédas, J.; Stuhr-Hansen, N.; Hedegård, P.; Bjørnholm, T. *Nature (London)* **2002**, *32*, 567–569.
- (46) Dewar, M. J. S.; Zoebish, E. G.; Healy, E. F.; Stewart, J. J. P. *J. Am. Chem. Soc.* **1985**, *107*, 3902–3909.
- (47) Ridley, J.; Zerner, M. *Theor. Chem. Acta* **1973**, *32*, 111–134.
- (48) Shemella, P.; Zhang, Y.; Mailman, M.; Ajayan, P.; Nayak, S. *Appl. Phys. Lett.* **2007**, *91*, 042101.
- (49) Hod, O.; Barone, V.; Scuseria, G. E. *Phys. Rev. B* **2008**, *77*, 035411.
- (50) Bader, R.; Chang, C. *J. Phys. Chem.* **1989**, *93*, 2946–2956.
- (51) Hehre, W.; Radom, L.; Pople, J. *J. Am. Chem. Soc.* **1972**, *94*, 1496–1504.
- (52) Zhang, Q.; Prins, P.; Jones, S. C.; Barlow, S.; Kondo, T.; An, Z.; Siebbeles, L. D. A.; Marder, S. R. *Org. Lett.* **2005**, *7*, 5019–5022.
- (53) Kikuzawa, Y.; Mori, T.; Takeuchi, H. *Org. Lett.* **2007**, *9*, 4817–4820.
- (54) Wang, X.; Li, X.; Zhang, L.; Yoon, Y.; Weber, P. K.; Wang, H.; Guo, J.; Dai, H. *Science* **2009**, *324*, 768–771.
- (55) Bock, C. W.; Trachtman, M.; George, P. *J. Mol. Struct.-Theochem* **1985**, *122*, 155 – 172.
- (56) Campanelli, A. R.; Domenicano, A.; Ramondo, F. *J. Phys. Chem. A* **2003**, *107*, 6429–6440.
- (57) Krygowski, T.; Stepien, B. *Chem. Rev.* **2005**, *105*, 3482–3512.
- (58) Rissner, F.; Egger, D. A.; Natan, A.; Koerzdoerfer, T.; Kuemmel, S.; Kronik, L.; Zojer, E. *J. Am. Chem. Soc.* **2011**, *133*, 18634–18645.
- (59) The HOMO (LUMO) level of the $N=7$ H-terminated flake (D_{2h} point group) has B_{3u} (B_{2g}) symmetry. Within the A-B functionalization scheme, the flake symmetry reduces to C_{2h} and

consequently the HOMO (LUMO) becomes a A_u (B_g) state. It is worth recalling that the symmetry considerations reported here are for ideal unrelaxed systems. Structural optimization further lowers the symmetry of functionalized flakes and consequently locally affects also the molecular orbital distribution.

(60) Martin-Samos, L.; Bussi, G.; Ruini, A.; Molinari, E.; Caldas, M. J. *Phys. Rev. B* **2010**, *81*, 081202.

(61) Cocchi, C.; Prezzi, D.; Ruini, A.; Benassi, E.; Caldas, M. J.; Corni, S.; Molinari, E. *J. Phys. Chem. Lett.* **2012**, *3*, 924–929.

SUPPORTING INFORMATION

Electronics and Optics of Graphene Nanoflakes: Edge Functionalization and Structural Distortions

Caterina Cocchi,^{*,†,‡} Deborah Prezzi,^{*,†} Alice Ruini,^{†,‡} Marilia J. Caldas,[¶] and
Elisa Molinari^{†,‡}

*Centro S3, CNR-Istituto Nanoscienze, I-41125 Modena, Italy, Dipartimento di Fisica, Università
di Modena e Reggio Emilia, I-41125 Modena, Italy, and Instituto de Física, Universidade de São
Paulo, 05508-900 São Paulo, SP, Brazil*

E-mail: caterina.cocchi@unimore.it; deborah.prezzi@unimore.it

*To whom correspondence should be addressed

[†]Centro S3, CNR-Istituto Nanoscienze, I-41125 Modena, Italy

[‡]Dipartimento di Fisica, Università di Modena e Reggio Emilia, I-41125 Modena, Italy

[¶]Instituto de Física, Universidade de São Paulo, 05508-900 São Paulo, SP, Brazil

The Supporting Information is organized in three sections. In the first one we report the structural details (bond lengths and distortion angles) of the optimized $N=7$, $N=8$ and $N=9$ graphene nanoflakes (GNFs), to complete the data reported in the main text. The second section supports the analysis on the electronic properties, including a table with the dipole moment components of $N=8$ and $N=9$ GNFs (functionalized according to both A-A and A-B schemes) and the isosurfaces of the frontier orbitals for the considered systems. The last part is dedicated to optical properties. The analysis on the effects related to different functionalization schemes and structural distortions are extended here also to COCH_3 and F terminations, as representatives of the classes of C-bonded and halogen substituents. We also include the tables with the composition of the main excitations for $N=8$ and $N=9$ GNFs, and the analysis of the optical features of full halogen-terminated GNFs (only $N=7$).

Structural Properties

We report in Table S1 and Table S2 the bond lengths – C-C and C-X bonds, respectively, with $X=\text{F, Cl, Br, N, O, C}$, depending on the functional group – at the edge of functionalized graphene nanoflakes (GNFs).

Table S1: C-C bond length (in Å) at the edge of each considered functionalized GNF, optimized with AM1 model. The case of H termination is also reported as a reference.

C-C bond length									
H	Halogens			Direct bond			C-bond		
	F	Cl	Br	NH_2	OCH_3	$\text{OCF}=\text{CF}_2$	COCH_3	$\text{CH}=\text{CH}_2$	$\text{CH}=\text{CF}_2$
1.40	1.38	1.38	1.38	1.40	1.38	1.37	1.38	1.38	1.38

Table S2: Bond lengths (in Å) between edge C atoms and functional groups for each considered functionalization.

Halogen			Direct bond			C bond		
F	Cl	Br	N	O		C		
				OCH_3	$\text{OCF}=\text{CF}_2$	COCH_3	$\text{CH}=\text{CH}_2$	$\text{CH}=\text{CF}_2$
1.39	1.70	1.88	1.40	1.38	1.40	1.49	1.46	1.45

In Table S3 we report the values of the distortion angle α for $N=8$ and $N=9$ functionalized

GNFs with selected substituents (F, NH₂ and COCH₃) for both A-A and A-B schemes. As introduced in the main text, α is defined as the maximum deviation from planarity of edge C atoms in functionalized GNFs. By inspecting Table S3 we notice that in general, as discussed for $N=7$ GNFs in the main text, larger distortions are noticed also for $N=8$ and $N=9$ GNFs in the schemes corresponding to lower symmetry models (A-B and A-A, respectively).

Table S3: Distortion angle α , expressed in degrees, of optimized GNFs of width parameter $N=8$ and $N=9$, functionalized with selected groups (F, NH₂ and COCH) according to both schemes. For F termination, the case of full functionalization is also addressed. The angle α represents the maximum deviation of edge C atoms from the planar configuration of the reference H-terminated flake.

	$N=8$			$N=9$		
	F	NH ₂	COCH ₃	F	NH ₂	COCH ₃
A-A	7.2	17.8	12.5	9.4	24.7	9.3
A-B	36.8	38.4	22.2	4.9	10.1	13.5
full	9.0	-	-	21.4	-	-

Electronic Properties

In Table S4 we report the components of the dipole moments of functionalized GNFs of width parameters $N=8$ and $N=9$ for both A-A and A-B scheme. As discussed in the main text, we notice that in general a non negligible dipole component along the longitudinal axis (μ_x) appears in the scheme corresponding to the lower nominal symmetry (A-B for $N=8$ and A-A for $N=9$). The sign of μ_x is determined by the electronegativity of the substituents. The results are basically in agreement with those discussed in the main text for $N=7$.

Table S4: Dipole components of functionalized GNFs of width parameter $N=8$ and $N=9$: one substituent per class is considered for both A-A and A-B schemes.

	Group	Scheme	μ_x [D]	μ_y [D]	μ_z [D]
$N=8$	F	A-A	0.005	-0.001	-0.819
		A-B	1.212	0.299	0.675
	NH ₂	A-A	-0.260	-0.081	0.116
		A-B	-16.317	-0.168	-0.691
	COCH ₃	A-A	-1.964	1.536	-0.414
		A-B	8.190	0.240	-0.191
$N=9$	F	A-A	7.409	0.002	0.076
		A-B	0.000	0.008	0.187
	NH ₂	A-A	-2.815	0.260	-2.321
		A-B	-1.191	0.970	1.594
	COCH ₃	A-A	9.806	0.034	0.200
		A-B	-2.128	-1.914	0.105

We present the isosurfaces of the frontier orbitals of $N=7$ (Figure S1), $N=8$ and $N=9$ GNFs (Figure S2) for the functionalized systems analyzed in the main text. For consistency, A-B (A-A) scheme is addressed for flakes with odd (even) N .

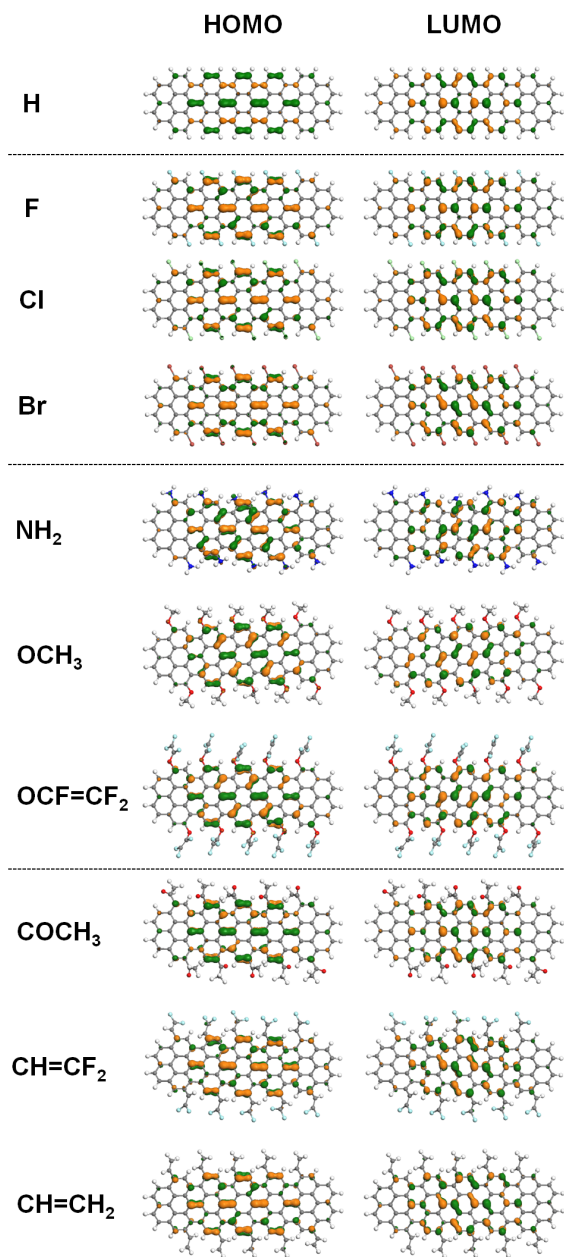


Figure S1: Isosurfaces of the frontier orbitals of functionalized GNFs ($N=7$) according to the A-B scheme. The orbitals of the reference H-terminated system are included for comparison.

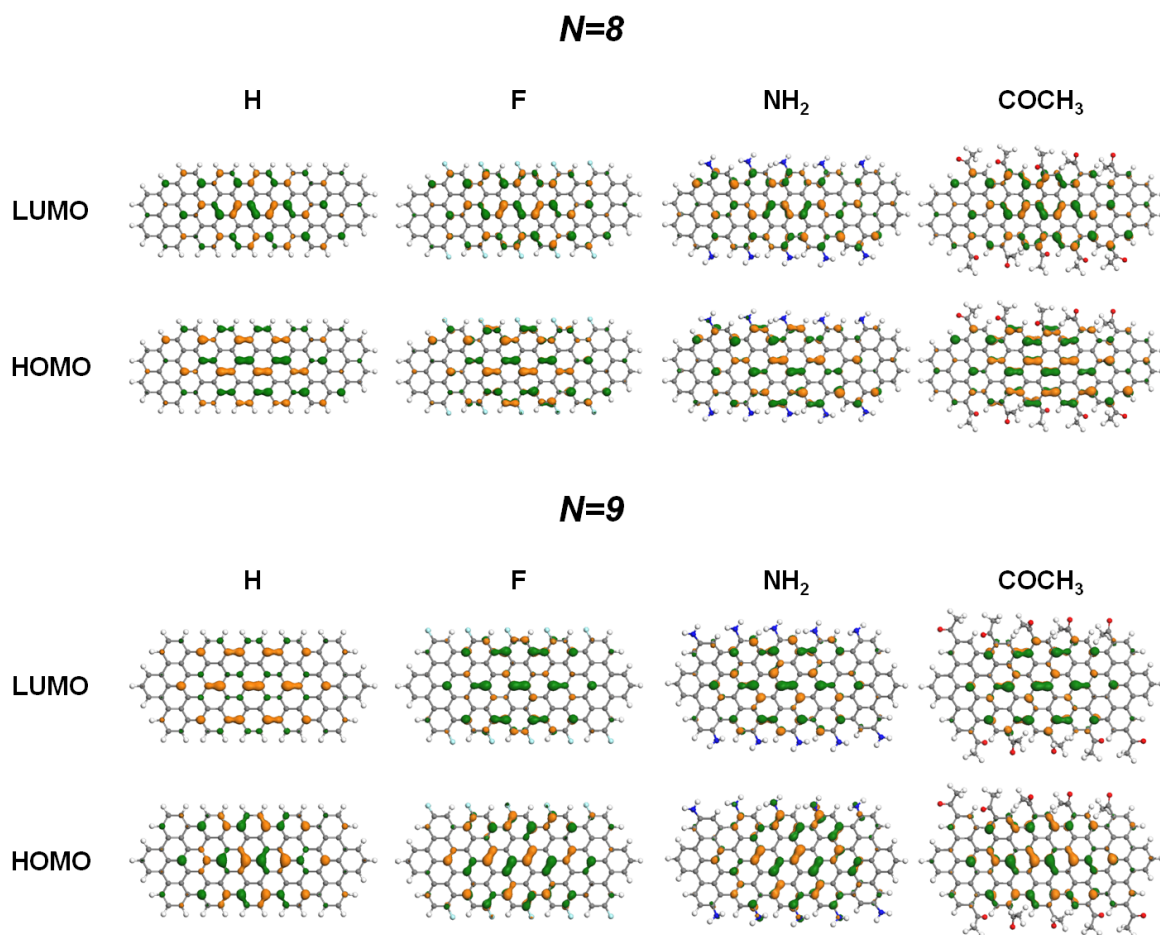


Figure S2: Isosurfaces of frontier molecular orbitals of functionalized GNFs of width parameters $N=8$ (*top*) and $N=9$ (*bottom*). The frontier orbitals of the reference H-terminated system are included for comparison. The A-A (A-B) scheme is addressed for $N=8$ ($N=9$).

Optical Properties

To supplement the analysis on functionalization-induced distortion effects on the optical properties of GNFs, we include in Figure S3 the optical spectra of $N=7$ GNFs, functionalized by means of COCH_3 groups [panels (a-b)] and F atoms [panels (c-d)]. In addition to the spectra of functionalized GNFs (solid lines), we include also those of the H-terminated distorted model structures, obtained by removing edge substituents from the final structure and then H-passivating the remaining dangling bonds (dashed lines); the spectrum of the reference H-terminated GNF is represented in the background of each panel (grey shaded area). Unlike NH_2 -functionalization (see also Figure 4 in the main text), here the spectra corresponding to the two schemes are basically identical for both substituent species, as suggested also from the similar geometry obtained in the two cases (see main text, Figure 2b for COCH_3 , and the values of the distortion angle α in Table 1). Compared to the reference H-GNF, we notice for all the spectra a red shift of P1 (about 150 meV) and of P2 (about 100 meV). Most part of these red shift effects (about 80%) is to be ascribed to structural distortions, as shown by the dashed spectra of the H-terminated distorted model flakes.

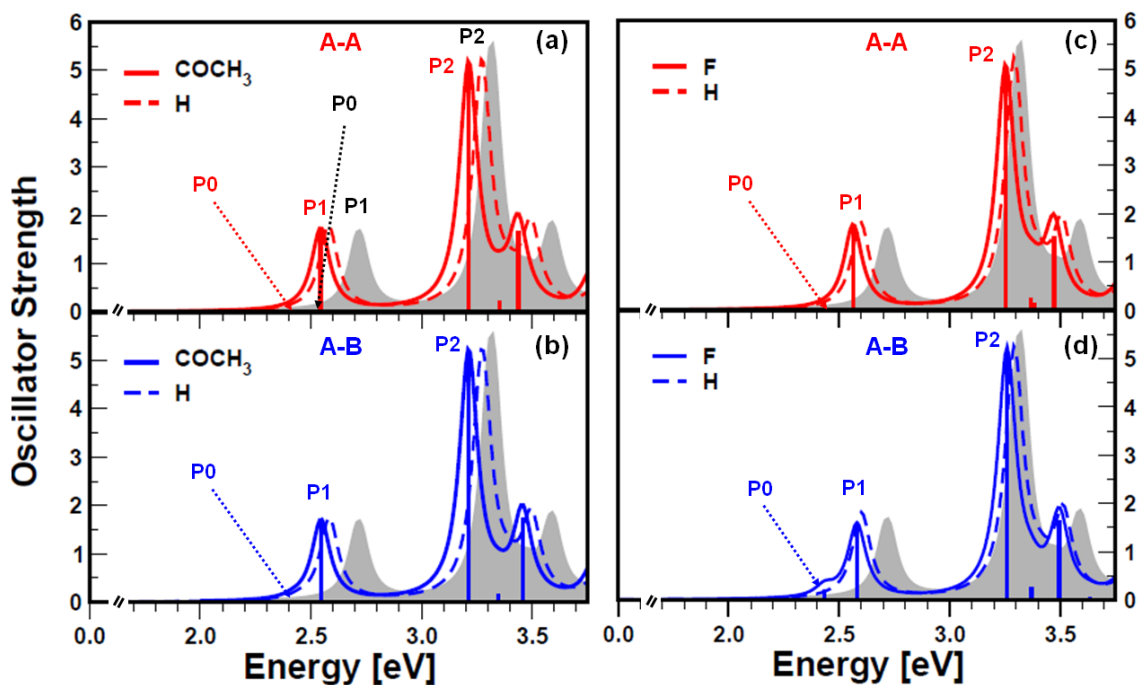


Figure S3: Optical spectra of GNFs of width parameter $N=7$, functionalized with COCH_3 (a-b) and F (c-d), according to the A-A and A-B schemes. In addition to the spectrum of the planar H-terminated flake taken as reference [grey shaded area, with the main excitations highlighted in (a)], we show the spectrum of model GNFs obtained by removing the edge substituents from the final structures and H-passivating the dangling bonds (dashed lines), in order to perform a rigorous analysis of distortions effects.

In Table S5 and Table S6 we report the composition of the main excitations of functionalized GNFs of width parameters $N=8$ and $N=9$, respectively. The corresponding spectra are shown in the main text (Figure 6).

Table S5: Energy, oscillator strength (OS) and composition of the two lowest energy excitations of functionalized GNFs of width parameter $N=8$ (A-A scheme, see spectra in Figure 6a of the main text). In the last column only the molecular orbital transitions with relative weights larger than 0.1 are reported.

System	Excitation	Energy [eV]	OS	Transitions (weight)
H	P1	1.84	3.33	H \rightarrow L (0.91)
	P2	3.64	3.47	H-2 \rightarrow L+2 (0.56)
F	P1	1.76	3.22	H \rightarrow L (0.91)
	P2	3.56	3.62	H-2 \rightarrow L+2 (0.62)
NH ₂	P1	1.69	3.04	H \rightarrow L (0.91)
	P2	3.04	1.64	H-2 \rightarrow L (0.46) H \rightarrow L+2 (0.18) H \rightarrow L+4 (0.15)
COCH ₃	P1	1.73	3.22	H \rightarrow L (0.91)
	P2	3.14	1.08	H-2 \rightarrow L+1 (0.23) H-2 \rightarrow L (0.10) H \rightarrow L+4 (0.26) H \rightarrow L+6 (0.13)

Table S6: Energy, oscillator strength (OS) and composition of the two lowest energy excitations of functionalized GNFs of width parameter $N=9$ (A-B scheme, see spectra in Figure 6b of the main text). In the last column only the molecular orbital transitions with relative weights larger than 0.1 are reported.

System	Excitation	Energy [eV]	OS	Transitions (weight)
H	P0	2.40	0.00	H-1 \rightarrow L (0.37) H \rightarrow L+1 (0.41)
	P1	2.47	1.71	H \rightarrow L (0.85)
	P2	3.24	4.47	H-2 \rightarrow L+2 (0.12) H-1 \rightarrow L+1 (0.73)
F	P0	2.34	0.06	H-1 \rightarrow L (0.36) H \rightarrow L+1 (0.39)
	P1	2.48	1.31	H \rightarrow L (0.78)
	P2	3.12	4.80	H-1 \rightarrow L+1 (0.69)
NH ₂	P1	2.17	0.76	H \rightarrow L (0.55) H \rightarrow L+1 (0.12)
	P0	2.44	0.50	H-1 \rightarrow L (0.27) H \rightarrow L (0.24) H \rightarrow L+1 (0.33)
	P2	3.03	4.64	H-1 \rightarrow L+1 (0.57)
COCH ₃	P0	2.33	0.01	H-1 \rightarrow L (0.37) H \rightarrow L+1 (0.41)
	P1	2.48	1.21	H \rightarrow L (0.80)
	P2	3.08	4.55	H-1 \rightarrow L+1 (0.64)

We finally present the results on the optical properties of fully functionalized $N=7$ GNFs with halogen terminations. In Figure S4(a) we show the computed spectra, where the main excitations are indicated for the reference H-GNF (grey shaded area). In case of full functionalization the model symmetry of the H-terminated flake is preserved and hence the character of the frontier orbitals [see Figure S4(b)] as well as the composition of the main excitations in terms of molecular orbital transitions and their intensity are not significantly affected (see Table S7). A red shift of the spectra (about 350 meV for P1 and about 250 meV for P2) is noticed, compared to the reference H-GNF.

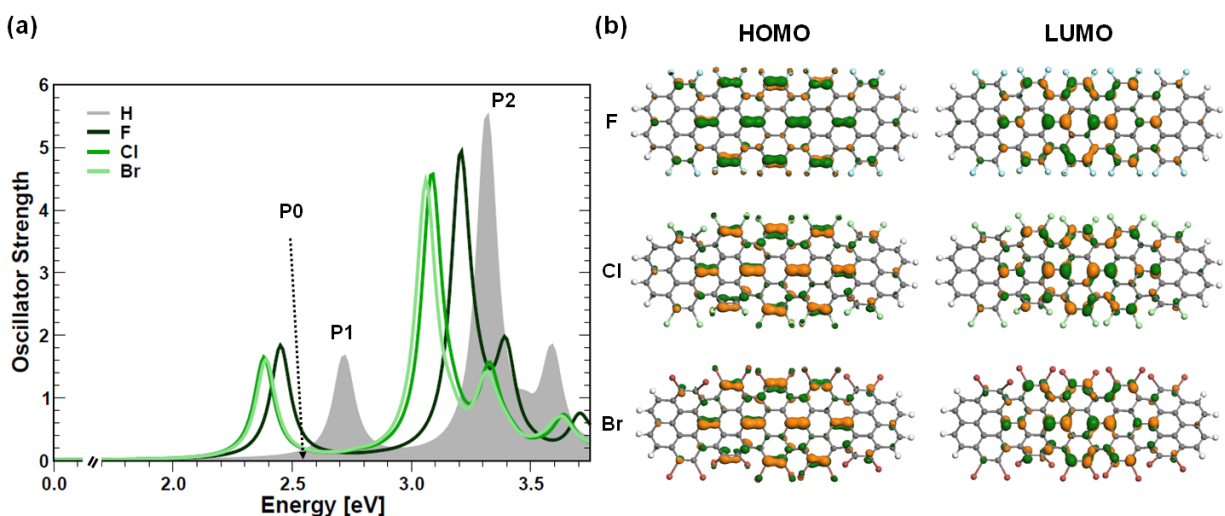


Figure S4: (a) Optical spectra of $N=7$ graphene nanoflakes fully functionalized with halogen atoms. For comparison, the spectrum of the reference H-terminated flake is included (grey shaded area with the labels of the main excitations). (b) Frontier orbitals of the corresponding structures.

Table S7: Energy, oscillator strength (OS) and composition of the main excitations (P0, P1 and P2) of fully functionalized $N=7$ GNFs with halogen terminations (F, Cl, Br – see Figure S5). In the last column only the molecular orbital transitions with relative weights larger than 0.1 are reported.

System	Excitation	Energy [eV]	OS	Transitions (weight)
H	P0	2.54	0.0005	H-1 \rightarrow L (0.37) H \rightarrow L+1 (0.39)
	P1	2.72	1.62	H \rightarrow L (0.79)
	P2	3.32	5.43	H-3 \rightarrow L+3 (0.12) H-1 \rightarrow L+1 (0.76)
F	P0	2.36	0.02	H-1 \rightarrow L (0.30) H \rightarrow L+1 (0.45)
	P1	2.45	1.81	H \rightarrow L (0.82)
	P2	3.21	4.70	H-3 \rightarrow L+3 (0.11) H-2 \rightarrow L+1 (0.73)
Cl	P0	2.27	0.01	H-1 \rightarrow L (0.28) H \rightarrow L+1 (0.42)
	P1	2.38	1.62	H \rightarrow L (0.81)
	P2	3.08	4.42	H-3 \rightarrow L+2 (0.10) H-1 \rightarrow L+1 (0.67)
Br	P0	2.27	0.01	H-1 \rightarrow L (0.29) H \rightarrow L+1 (0.42)
	P1	2.39	1.59	H \rightarrow L (0.81)
	P2	3.06	4.33	H-3 \rightarrow L+2 (0.10) H-1 \rightarrow L+1 (0.69)